



Virtual craniofacial reconstruction using computer vision, graph theory and geometric constraints

Ananda S. Chowdhury^{a,*}, Suchendra M. Bhandarkar^a, Robert W. Robinson^a, Jack C. Yu^b

^a Department of Computer Science, The University of Georgia, Athens, GA 30602, USA

^b Department of Plastic Surgery, The Medical College of Georgia, Augusta, GA 30912, USA

ARTICLE INFO

Article history:

Received 30 January 2008

Received in revised form 24 February 2009

Available online 25 March 2009

Communicated by G. Borgefors

Keywords:

ICP

Bipartite graph matching

Graph automorphism

Hausdorff distance

Computed Tomography

ABSTRACT

A novel solution to the problem of virtual craniofacial reconstruction using computer vision, graph theory and geometric constraints is proposed. Virtual craniofacial reconstruction is modeled along the lines of the well-known problem of rigid surface registration. The Iterative Closest Point (ICP) algorithm is first employed with the closest set computation performed using the Maximum Cardinality Minimum Weight (MCMW) bipartite graph matching algorithm. Next, the bounding boxes of the fracture surfaces, treated as cycle graphs, are employed to generate multiple candidate solutions based on the concept of graph automorphism. The best candidate solution is selected by exploiting local and global geometric constraints. Finally, the initialization of the ICP algorithm with the best candidate solution is shown to improve surface reconstruction accuracy and speed of convergence. Experimental results on Computed Tomography (CT) scans of real patients are presented.

© 2009 Elsevier B.V. All rights reserved.

1. Introduction

In fast-paced modern society, craniofacial fractures, especially mandibular fractures, are very frequently encountered, most often due to gunshot wounds, motor vehicle accidents and sports-related injuries (King et al., 2004). The resulting craniofacial and mandibular fractures exhibit certain distinct patterns. Sometimes, these patterns imply a single fracture, and, in some other cases, a combination of single fractures (Ogundare et al., 2003). From a surgical standpoint, the fractures are fixated one at a time in the operating room and hence must be so handled in the pre-surgical planning phase as well. Thus, reconstruction of a single mandibular fracture assumes paramount importance in almost all cases. The proposed scheme for computer vision guided virtual craniofacial reconstruction from a sequence of Computed Tomography (CT) images allows the surgeon to reconstruct accurately the fractured craniofacial skeleton *in silico* before performing the surgery *in vivo*.

The above reconstruction problem is also one of general interest from the perspectives of computer vision and pattern recognition. The input to the problem is a sequence of 2D slices showing a fractured human mandible with two broken fragments. The goal

is to register these broken fragments with the transformation, derived from registering their fractured surfaces. Having cast the problem as one of rigid registration, the well-known Iterative Closest Point (ICP) algorithm (Besl and McKay, 1992) is employed to match the fracture surfaces by matching the points on them. A fracture surface can be also considered, in the present scenario, to have a bounding box. We next match the fracture surfaces by matching their bounding boxes based on certain geometric constraints. We call this the Geometric algorithm. Finally, the combination of the ICP and the Geometric algorithms, termed as the Geometric-ICP algorithm, is shown to yield a faster as well as a more accurate solution. Graph matching and graph automorphism are respectively used to establish the correspondence and limit the number of initial states for the ICP algorithm. The remainder of the paper is organized as follows. In Section 2, we discuss the current state of the art and highlight our contribution. Section 3 discusses the underlying theoretical foundations of our work. Section 4 describes the basic image processing operations. Section 5 discusses the ICP-based reconstruction algorithm. Sections 6 and 7, respectively explore graph automorphism for generation of multiple initial states for the ICP algorithm and selection of the best initial state based on local and global geometric constraints. In Section 8, Geometric and hybrid Geometric-ICP algorithms are proposed as alternative methods of reconstruction. Section 9 presents the experimental results and their analysis on CT scans of real patients. Finally, the paper is concluded in Section 10 with an outline of future work.

* Corresponding author. Address: Jadavpur University, Department of Electronics and Telecommunication Engineering, 188, Raja S.C. Mallik Road, Jadavpur, Calcutta 700032, India. Tel.: +91 33 2414 6666; fax: +91 33 2414 6217.

E-mail addresses: ananda.chowdhury@gmail.com (A.S. Chowdhury), suchi@cs.uga.edu (S.M. Bhandarkar), rwr@cs.uga.edu (R.W. Robinson), jyu@mcc.edu (J.C. Yu).

2. Literature review and our contribution

While there is recent work in the literature dealing with simulation of mandibular fractures (Nakajima et al., 2001) and simulation of dental implantology (Siessegger et al., 2001), there is little reported by way of automated computer-aided surgical reconstruction of the craniofacial skeleton in recent years. Patel et al. (1996) have examined the issues involved in computer-assisted craniofacial surgical planning and simulation using CT, computer visualization and graphical simulation techniques. Cevidanes et al. (2007) have described image processing methods for the computation of morphometric changes associated with jaw surgery. Enciso et al. (2003) and Mollemans et al. (2005) have examined issues pertaining to soft tissue modeling and simulation of jaw motion in the context of craniofacial surgery. The Iterative Closest Point (ICP) (Besl and McKay, 1992) algorithm is observed to be a popular computer vision algorithm for surface registration in the field of medical imaging (Granger et al., 2001). Bhandarkar et al. (2007a) have proposed a synergistic combination of the Data Aligned Rigidity Constrained Exhaustive Search (DARCES) and the ICP algorithms for solving the problem of virtual craniofacial reconstruction. The focus of the work was on outlier rejection to give the ICP algorithm a better initial starting solution. No work, to the best of our knowledge, has thus far been reported on the exploration of graph automorphism and enforcement of different types of geometric constraints to improve the performance of the ICP algorithm.

Our contribution in this paper is twofold. From an application standpoint, a biomedical imaging problem of critical importance to practicing surgeons is successfully explored. From computer vision and pattern recognition perspectives, we show how (a) bipartite graph matching can be used to compute the closest set in the ICP algorithm, (b) automorphisms of cycle graphs can be employed as a meaningful alternative to generate multiple initial states for the ICP algorithm, and (c) local and global geometric constraints can be utilised to select the best initial state and eventually improve the accuracy and speed of convergence of the ICP algorithm. A preliminary version of the paper was presented in (Bhandarkar et al., 2007b).

3. Theoretical foundations

In this section, we present some basic definitions and concepts pertaining to types of graphs, graph matchings and graph automorphisms, which will be exploited later in the paper. For further details, the interested reader is referred to standard textbooks on graph theory such as (Papadimitriou and Steiglitz, 1982; Christofides, 1975 and Valiente, 2002):

Definition 1. A graph G is an ordered pair of disjoint sets (V, E) such that E is a subset of the set $V^{(2)}$ of unordered pairs of V . The set V is the set of vertices and E is the set of edges.

Definition 2. The order of G is the number of vertices in G and the size of G is the number of edges in G .

Definition 3. A graph $G(V_1 \cup V_2, E)$ is bipartite if the two vertex sets V_1 and V_2 are disjoint and every edge in the edge set E joins a vertex of V_1 to a vertex of V_2 .

Definition 4. A walk W in a graph G consists of an alternating sequence of vertices and edges, say $(v_0, e_1, v_2, e_2, \dots, v_n, e_n)$, where $e_i = \{v_{i-1}, v_i\}$, $0 < i \leq n$. W is termed a $v_0 - v_n$ walk and is denoted by $v_0 v_1 \dots v_n$; the length of W is n .

Definition 5. A graph C_n constitutes a cycle of order n if its vertices v_i , $0 < i \leq n$, are distinct from each other, $n \geq 3$, $v_0 = v_n$, and there exists a walk $v_0 v_1, \dots, v_n$ which contains all the edges of C_n .

Definition 6. A cycle graph is a graph that consists of a single cycle.

Definition 7. A matching M of a graph $G = (V, E)$ is a subset of the edges with the property that no two edges of M share a common vertex.

Definition 8. If edge weights are given by a function $w : E \rightarrow \mathbb{R}^+$ the weight of a matching is defined as $w(M) = \sum_{e \in M} w(e)$. The Maximum Weight Matching problem is to determine a matching M in G that has maximum weight.

Definition 9. When the cardinality of a matching is $|V|/2$ in a graph with $|V|$ nodes, we say the matching is complete or perfect. In order to have a perfect matching, the order of the graph has to be even.

Definition 10. If the edge weights of a graph are all unity, the matching problem essentially becomes a Cardinality Matching problem. A Maximum Cardinality Matching is a matching with the maximum possible number of edges.

Definition 11. Two graphs $G_1 = (V_1, E_1)$ and $G_2 = (V_2, E_2)$ are isomorphic, denoted by $G_1 \cong G_2$, if there exists a bijection $M \subseteq V_1 \times V_2$ such that, for every pair of vertices $v_i, v_j \in V_1$ and $w_i, w_j \in V_2$ with $(v_i, w_i) \in M$ and $(v_j, w_j) \in M$, $(v_i, v_j) \in E_1$ if and only if $(w_i, w_j) \in E_2$. In such a case M is a graph isomorphism from G_1 to G_2 .

Definition 12. An automorphism of a graph G is a graph isomorphism between G and itself.

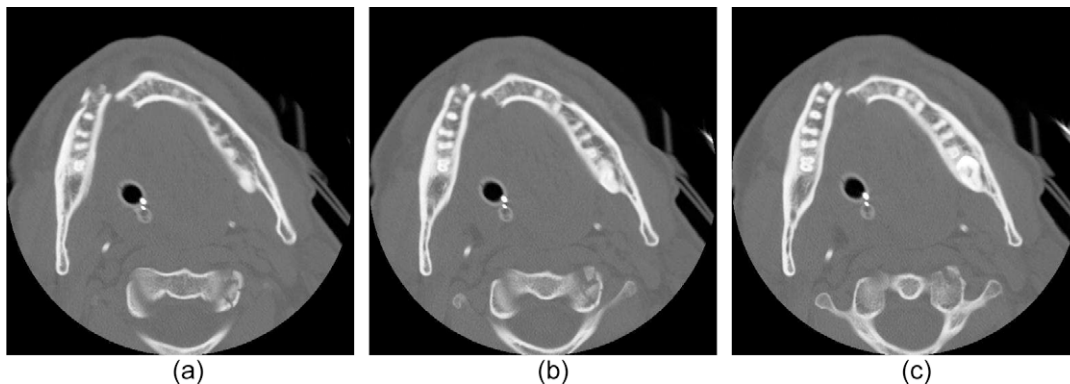


Fig. 1. A real patient CT image sequence of a fractured mandible. The images in (a), (b) and (c) are three consecutive slices in the CT sequence.

Definition 13. The set of all automorphs of a graph forms a group under the operation of composition. This group is termed the *automorphism group* of the graph.

Definition 14. The *order* of a group denotes the number of elements of that group.

4. Image processing operations

The input to the computer vision guided virtual craniofacial reconstruction system is a sequence of 2D grayscale images of a fractured human mandible, generated using CT. Fig. 1 is a CT image sequence obtained from a real (human) patient where the images shown in Fig. 1a–c represent three consecutive CT slices. A series of image processing tasks is undertaken before using the surface matching algorithms to register the two fractured bone fragments (Bhandarkar et al., 2007a). The result of the image processing operations on the real (human) patient CT slice in Fig. 1a is shown in Fig. 2. A brief description of the image processing operations is provided in the following subsections.

4.1. Thresholding

The selection of the appropriate threshold is not obvious since the CT images typically contain objects or artifacts of different intensities (i.e. varying Hounsfield unit values). For example, a fractured mandibular fragment could contain cavities, dental fillings, crowns and other dental prostheses. In such cases, entropy-based thresholding (Sahoo et al., 1988) was found to perform better than simple thresholding. In the case of entropy-based thresholding, the threshold value (represented by the variable T in equation (1)) is determined via maximization of the inter-class entropy computed from the grayscale histogram of the CT image. The entropy, in general, is a probabilistic measure of the uncertainty of an event. For an image, the entropy S_c for each grayscale class c (consisting of several grayscale values) can be computed using the grayscale histogram as follows:

$$S_c = \sum_{k \in G_c} p(k) \log_2(p(k)) \quad (1)$$

where $p(k)$ is the probability of a pixel having a grayscale value k and G_c is the set of grayscale values for class c . In the context of binarization, the grayscale threshold T is chosen such that the total entropy $S = \sum_{c=1}^2 S_c$ is maximized.

4.2. Connected component labeling

Binarization of the CT image by itself cannot extract reliably the two fracture fragments, as is evident from Fig. 2b. This is simply

because one still needs to filter out the undesired artifacts so that only the fractured mandibular fragments are used for the purpose of surface matching. A 2D Connected Component Labeling (CCL) procedure in conjunction with a component area filter was used to remove the undesired artifacts (which are typically small in size). Connected components with area less than a threshold value (chosen as 1000 pixels) are deleted. The result of these operations is illustrated in Fig. 2c. The results of the 2D CCL procedure are propagated across the CT image slices, resulting in a 3D CCL algorithm. A 3D component (a fractured jaw bone in this case) is identified by computing the area of overlap of the corresponding 2D components in successive CT image slices.

4.3. Contour data extraction

After performing the thresholding, CCL and size filtering operations on all the CT image slices, the task of interactive contour detection is performed on the resulting binary image slices. The user can click on potentially interesting points on a fracture contour (typically points of high curvature). The intervening fracture contour points are generated automatically by a contour following algorithm. A 3D surface point dataset is generated for each fracture surface by collating the individual fracture contour data points.

5. ICP-based reconstruction

In this section, we describe the process of virtual craniofacial reconstruction procedure using the ICP algorithm (Bhandarkar et al., 2007a). The task of the ICP algorithm (Besl and McKay, 1992) is twofold. The first part is to establish a correspondence between the two surface point sets to be matched. The second part is to compute a 3D transformation that brings the two sets into registration. In the present problem, the cardinalities of the two data sets to be matched are different. We term the fragment (dataset) to be matched the *sample* fragment (dataset) and the fragment (dataset) to which the sample fragment (dataset) is to be matched the *model* fragment (dataset). Let the sample and model fragments be denoted by frg_1 and frg_2 , respectively. By the term matching, in this context, we actually mean registration of the two fragments. It is important to note that each of the two broken fragments has a fractured surface (the sample fragment has sample fracture surface and the model fragment has a model fracture surface). We actually predict the 3D rigid body transformation needed to bring the sample fracture surface into registration with the model fracture surface. We then apply that 3D rigid body transformation to the entire sample fragment to register it with the model fragment.



Fig. 2. (a) A typical 2D CT slice (from a real patient CT sequence). (b) The CT slice after Entropy Thresholding. (c) The CT slice after Connected Component Labeling and Size Filtering. In (c), the two broken mandibular fragments are represented by two different intensity values.

5.1. The basic ICP algorithm

The basic ICP algorithm consists of the following steps:

1. The matching points in the model dataset corresponding to points in the sample dataset are determined. This new set of matching points in the model dataset, which represents a subset of the original model dataset, is termed the *closest set*.
2. The 3D rigid body transformation (3D translation and 3D rotation) that brings the two surfaces into registration is using the Theory of Quaternions (Hamilton, 1847).
3. The computed transformation is applied to the original sample dataset and the mean squared error (MSE) between the transformed sample data points and the corresponding points in the closest set is calculated. The MSE (ϵ^2) is given by:

$$\epsilon^2 = (1/n) \sum_{i=1}^n \left((c_i - (Rs_i + T))^2 \right) \quad (2)$$

where R denotes the rotation matrix, T denotes the translation vector, s_i denotes a point in the sample data set, c_i represents the corresponding point in the closest set and n is the total number of sample points.

Steps 1–3 are repeated with an updated sample dataset that is generated by applying R and T obtained in the current iteration to the current sample dataset. The algorithm is deemed to have converged when the difference in MSE between two successive iterations drops below a pre-specified threshold (0.01 mm² in our case).

5.2. Closest set computation

Graph theoretic matching has been used extensively in several computer vision problems (Kim and Kak, 1991). In the computation of the closest set, which is the most crucial step in the ICP algorithm, the matching point pairs are determined using the Maximum Cardinality Minimum Weight (MCMW) bipartite graph matching algorithm based on the Hungarian method proposed by Kuhn (1955). We construct a bipartite graph $G(V_1 \cup V_2, E)$ where the 3D sample and model datasets correspond to the two disjoint vertex sets V_1 and V_2 , respectively. The weight w_{ij} of an edge $e_{ij} \in E$ between two vertices $v_i = (x_i, y_i, z_i)$ and $v_j = (x_j, y_j, z_j)$ where $v_i \in V_1$ and $v_j \in V_2$ is given by the Euclidean distance between v_i and v_j :

$$w_{ij} = ((x_i - x_j)^2 + (y_i - y_j)^2 + (z_i - z_j)^2)^{1/2} \quad (3)$$

Theorem 1. *The worst-case time-complexity of the Maximum Cardinality Minimum Weight (MCMW) algorithm for a bipartite graph $G = (V_1 \cup V_2, E)$ with $|V_1| = |V_2| = n$ is $O(n^3)$.*

For a complete proof of the above theorem the interested reader is referred to (Papadimitriou and Steiglitz, 1982 and Christofides, 1975).

Theorem 2. *Given that in typical cases of craniofacial injury, the rotational or translational displacements are not very large, the Maximum Cardinality Minimum Weight (MCMW) algorithm for a bipartite graph correctly establishes the correspondence between two fracture surfaces at every stage of the Iterative Closest Point (ICP) algorithm in polynomial time.*

Proof. Our proof is based on Theorem 1. Each fracture surface, consisting of several 3D data points, is modeled as a vertex set of a weighted bipartite graph $G = (V_1 \cup V_2, E)$. The bipartite graph is complete, i.e., there exists an edge $e_{ij} \in E$ between each vertex pair (v_i, v_j) where $v_i \in V_1$ and $v_j \in V_2$. The weight w_{ij} of edge e_{ij} is

chosen to be the Euclidean distance between the corresponding vertices $v_i \in V_1$ and $v_j \in V_2$ where $i = 1, 2, \dots, n_1; n_1 = |V_1|$ and $j = 1, 2, \dots, n_2; n_2 = |V_2|$. Without the loss of generality, the vertex set with lower cardinality is called the *sample set* and the one with the higher cardinality is called the *model set*. The goal is to compute the *closest set*; i.e., a maximal subset of the model set wherein each point corresponds to a unique point in the sample set such that all points in the sample set are exhausted (in compliance with the principle of maximum cardinality) and simultaneously, the sum of the edge weights between all pairs of corresponding points (i.e., $\sum w_{ij}$) is minimized (in compliance with the principle of minimum weight). This procedure is carried out within each iteration of the ICP algorithm. In the case the of small or moderate translational or rotational displacements, this graph theoretic optimization procedure, with an objective function formulated as the *sum of the Euclidean distances between all the pairs of matched points*, correctly matches a sample point with a model point without distorting the shape of the fracture surfaces. A greedy approach (Cormen et al., 2001), based on the minimum Euclidean distance between individual pairs of points considered one at a time, on the other hand, would map more than one sample point to a single model point and distort the fracture surface shape. Our problem formulation maps to the following well-known Maximum Cardinality Minimum Weight (MCMW) Bipartite Graph Matching Problem in graph theory, i.e., given a weighted complete bipartite graph $G = (V_1 \cup V_2, E)$ with edge-weights $w_{ij} \geq 0$; determine a pairing of the vertices from two vertex sets V_1 and V_2 such that the vertex set with smaller cardinality is completely exhausted and the total cost of the pairings is a minimum. By virtue of its construction the proposed bipartite graph is complete with $E = V_1 \times V_2$. Here $|V_1| \leq |V_2|$; so the MCMW matching gives a 1:1 mapping of V_1 into V_2 . From Theorem 1, the MCMW algorithm runs in $O(n^3)$ time for a bipartite graph with two vertex sets of equal cardinality n . So, in our case it runs in time $O(n_1^3)$ since $n_1 \leq n_2$. Thus, the proposed solution clearly runs in polynomial time. \square

6. Graph automorphisms as initial ICP states

Besl and McKay (1992) have proposed multiple value initialization as a means to attain a global minimum in their version of the ICP algorithm. For two 3D datasets, they have suggested comparing the shape-based principal moments and sampling the quaternion states based on rotation groups of regular polyhedra to produce multiple initial starting states. In the present problem, the two 3D datasets, i.e., the two fracture surfaces, have well-defined geometric boundaries. Thus, we model each fracture surface bounding box as a cycle graph of order 4 and generate multiple solutions based on the automorphism group. The bounding box for the individual fracture surfaces is constructed by simply using two pairs of extreme points of a fracture contour that appear in the first and last image slice of the CT image sequence. Let us denote the cycle graph of the fracture surface of frg_1 by B_1 and that of frg_2 by B_2 . Since the two fracture surfaces behave as two rigid objects, their matching should guarantee the matching of their bounding boxes and vice-versa. It is a well-known fact that the graph isomorphism problem $\in \mathbf{NP}$, but it can be solved in **polynomial time** for many special graphs (Valiente, 2002). Now, we state and prove a result on graph automorphism for cycle graphs.

Theorem 3. *The automorphisms of a cycle graph C_n on $n \geq 3$ vertices form a group of order $2n$ (Valiente, 2002).*

Proof. A cycle graph C_n on $n \geq 3$ vertices is left fixed exactly by n rotations and exactly by n reflections. Thus, the resulting automorphism group has order $2n$. \square

From Theorem 3, it is clear that the generation of automorphs for a cycle graph of order n has time-complexity $O(n)$. Since the automorphism group of, say, B_2 consists of 4 rotation members and 4 reflection members, there can be only 8 possible competing orientations of B_2 to match with B_1 . We denote the l th automorph of B_2 by $AB_{2,l}$ where $l = 1, \dots, 8$. Thus, in the case of the present problem, the number of initial ICP states is shown to be limited by the above result from graph automorphisms.

7. Best initial state selection

After the total number of initial solutions is determined, we apply local and global geometric constraints to select the best initial solution. Note that the MCMW bipartite graph matching algorithm essentially establishes the correspondence between the points on the two opposite fracture surfaces and that no geometric constraints have been applied so far. We use two local geometric constraints, namely, (a) the lengths of the sides, and (b) angles between pairs of sides of the bounding boxes of the fracture surfaces. By the term *global geometric constraint*, we refer to the overall shape of the mandible.

7.1. Local geometric constraints

Kim and Kak (1991) have shown how local geometric constraints can be exploited to improve the correspondence obtained via bipartite graph matching in the context of object recognition. We introduce a dissimilarity function based on two geometric constraints which are invariant under rigid body transformation. In order for B_1 and $AB_{2,l}$ to be well matched:

1. The lengths of corresponding pairs of sides of B_1 and $AB_{2,l}$ should be well matched. Let us denote the lengths of the i th sides of B_1 and $AB_{2,l}$ by d_i^1 and $d_i^{2,l}$, respectively.
2. The angles between the corresponding pairs of sides of B_1 and $AB_{2,l}$ should also be well matched. Let us denote the angle bounded by sides i and j of B_1 and $AB_{2,l}$ by θ_{ij}^1 and $\theta_{ij}^{2,l}$, respectively.

Let the 4 vertices of B_1 and $AB_{2,l}$ be denoted by (v_1^1, \dots, v_4^1) and $(v_1^{2,l}, \dots, v_4^{2,l})$. Each vertex can be considered a point in 3D space e.g. v_1^1 has coordinates xv_1^1, yv_1^1, zv_1^1 etc. Then d_i^k (where $k = 1, (2, l)$ and $i = 1, \dots, 4$) is given by:

$$d_i^k = \left[\left(xv_i^k - xv_{((i \bmod 4) + 1)}^k \right)^2 + \left(yv_i^k - yv_{((i \bmod 4) + 1)}^k \right)^2 + \left(zv_i^k - zv_{((i \bmod 4) + 1)}^k \right)^2 \right]^{1/2} \quad (4)$$

Likewise, θ_{ij}^k (where $k = 1, (2, l)$, $i = 1, \dots, 4$ and $j = 1, \dots, 4$) can be written as:

$$\theta_{ij}^k = \arccos \left(\left(\vec{d}_i^k \cdot \vec{d}_j^k \right) / \left(|\vec{d}_i^k| |\vec{d}_j^k| \right) \right) \quad (5)$$

The dissimilarity function $\Gamma(B_1, AB_{2,l})$ between B_1 and the l th member of AB_2 can now be defined as a linear combination of the above factors:

$$\begin{aligned} \Gamma(B_1, AB_{2,l}) &= \lambda_1 \Gamma_1(B_1, AB_{2,l}) + \lambda_2 \Gamma_2(B_1, AB_{2,l}), \text{ where} \\ \Gamma_1(B_1, AB_{2,l}) &= \sum_{i=1}^4 \left(|d_i^1 - d_i^{2,l}| \right), \text{ and} \\ \Gamma_2(B_1, AB_{2,l}) &= \sum_{i=1}^4 \left(\left| \theta_{i,((i \bmod 4) + 1)}^1 - \theta_{i,((i \bmod 4) + 1)}^{2,l} \right| \right) \end{aligned} \quad (6)$$

The values of λ_1 and λ_2 are determined from the variations of the terms $\Gamma_1(B_1, AB_{2,l})$ and $\Gamma_2(B_1, AB_{2,l})$ for 8 possible values of l and from the normalization constraint $\lambda_1 + \lambda_2 = 1$. The dissimilarity

function is computed between B_1 and each of the automorphs of AB_2 . The lower the value of the dissimilarity function $\Gamma(B_1, AB_{2,l})$, the better is the match between B_1 and $AB_{2,l}$. The 8 automorphs are ranked in ascending order of their $\Gamma(B_1, AB_{2,l})$ values and the top 50% i.e. first 4 automorphs are chosen as the more suitable candidates for being opposable to B_1 .

7.2. Global geometric constraints

Wang et al. (2000) have used geodesics and knowledge of local geometry to improve surface correspondence. We apply the knowledge of the global geometric constraint, i.e. the shape of the mandible, to determine the best initial solution for the ICP algorithm. The transformation between B_1 and each of the 4 eligible automorphs of B_2 (as determined in Section 7.1) is estimated. The two broken fragments frg_1 and frg_2 are registered in 4 different ways using these transformations. Although the registration problem at hand is essentially a 3D one, we chose the central 2D slice of the coarsely registered mandible (from all 4 cases) and compared its shape with an unbroken reference mandible appearing in central 2D CT image slice. We could have also compared the 3D shape of the intact reference mandible with each of these four reconstructed mandibles. To simplify the matter without incurring any error, we decided to compare the central 2D CT slices, which faithfully capture the shapes of the intact reference mandible and the coarsely registered mandibles. The contours Co_1, \dots, Co_4 of each of the reconstructed mandibles and contour Co_{ref} of the intact reference mandible are extracted using simple edge detection. Contour-based shape similarity measures have been well explored in the computer vision literature (e.g., see Veltkamp and Latecki, 2006). We have chosen Hausdorff distance as the measure for the contour-based shape similarity for the present problem because its relatively fast $O(mn)$ time complexity (where m and n denotes numbers of points on the two contours under consideration), and because it circumvents the need to establish a prior correspondence between the pixels on the two contours under consideration. The bounding box for each of the five contours is determined. The contours are appropriately scaled so that their corresponding bounding boxes match each-other. The Contour Hausdorff Distance (CHD) between two scaled contour data sets Co_i^s (where $i = 1, \dots, 4$) and Co_{ref}^s is given by (Huttenlocher et al., 1993):

$$H(Co_i^s, Co_{ref}^s) = \max \left(h(Co_i^s, Co_{ref}^s), h(Co_{ref}^s, Co_i^s) \right) \quad (7)$$

where $h(Co_i^s, Co_{ref}^s)$ is the directed Hausdorff distance between the two data sets Co_i^s and Co_{ref}^s and is defined as:

$$h(Co_i^s, Co_{ref}^s) = \max_{a \in Co_i^s} \min_{b \in Co_{ref}^s} \|a - b\| \quad (8)$$

Here $\|a - b\|$ represents the Euclidean distance between the points a and b . The contour that yields the minimum value of CHD is deemed to be the best matching contour. In this manner, the best automorph of AB_2 and the best coarse transformation that registers two fracture surfaces using their bounding boxes are obtained.

8. Geometric and Geometric-ICP algorithms

We refer to the algorithm which registers the two fracture surfaces based on their bounding boxes as the Geometric algorithm. The term ‘‘Geometric’’ is justified since the algorithm satisfies the relevant local and global geometric constraints. Next, we propose a hybrid Geometric-ICP algorithm by exploiting the synergy between the Geometric algorithm and the ICP algorithm. Let the transformations determined by the Geometric, ICP and Geometric-ICP algorithms be denoted by ϕ_G, ϕ_{ICP} and ϕ_{GICP} , respectively so that:

Table 1
Dissimilarity function values for the competing best 4 automorphs.

Rank of the automorph	Value of the dissimilarity function
1	52.20
2	57.30
3	61.37
4	66.51

$$[\phi_{GICP}] = [\phi_G][\phi_{ICP}] \quad (9)$$

The ICP algorithm can yield an accurate 3D rigid-body transformation. However, it is sensitive to the initial starting point. In the context of the present rigid-body registration problem, the two fracture surfaces have definite geometric boundaries. The ICP algorithm can register the two fracture surfaces but lacks the direct enforcement of geometric constraints. The Geometric algorithm, on the other hand, enforces the necessary local and global geometric constraints, but the matching is based exclusively on the vertices of the bounding boxes of the two fracture surfaces. Hence, the Geometric algorithm lacks the iterative refinement capability of the ICP algorithm. However, it is important to note that the transformation resulting from the Geometric algorithm can provide an excellent starting point for the ICP algorithm. Since the proposed Geometric-ICP algorithm (where the output of the Geometric algorithm is used to initialize the ICP algorithm) is initialized with a geometrically correct initial starting point, it is expected to result in a higher registration accuracy along with a faster rate of convergence.

9. Experimental results and analysis

We have chosen five CT image sequences, obtained from the Department of Radiology at the Medical College of Georgia, for the purpose of experimentation. As our main emphasis is to illustrate the reduction in the registration error, we show the MSE for all 3 algorithms, for all 5 datasets in Table 3. For other details, such as the image processing tasks, selection of the best automorph *etc.*, we show the results for dataset 1. The CT image sequence, shown in Fig. 1, is representative of a class of fracture of its kind. The results of the image processing tasks are displayed in Fig. 2. Let the vertices of the bounding box B_1 be denoted by $M-N-O-P$ and

Table 2
CHD values for competing contours.

Contour from Fig. 3	Rank	Value of the Contour Hausdorff Distance (CHD)
Column 1, Row 2	3	111.22
Column 2, Row 2	1	2.24
Column 3, Row 2	2	52.43
Column 4, Row 2	4	149.97

those of B_2 by $P-Q-R-S$. Then the members of the automorphism group of B_2 are given by:

1. $P-Q-R-S, S-P-Q-R, R-S-P-Q, Q-R-S-P$ (4 rotational automorphs).
2. $Q-P-S-R, P-S-R-Q, S-R-Q-P, R-Q-P-S$ (4 reflectional automorphs).

The top 50%, *i.e.*, 4 out of 8, automorphs are selected based on the value of the dissimilarity function $\Gamma(B_1, AB_{2,i})$ (Eq. (6)). The values of the dissimilarity function for the best 4 automorphs are shown in Table 1.

The dissimilarity function values of the best 4 automorphs are observed to be very close (Table 1). This justifies the imposition of global constraint to finally select the best candidate automorph. Contours of the reference mandible and those of the 4 coarsely registered mandibles are shown in Fig. 3. The values of the CHD, used as a measure of global shape matching are shown in Table 2.

Fig. 3 and Table 2 indicate clearly that there is a single prominent winner among the 4 competing automorphs. Visually speaking, only one of the coarsely registered contours resembles the reference contour. From a quantitative standpoint, the CHD value of one of the contours is observed to be extremely low compared to the CHD values of the other three. Note that the fact that the reference intact mandible used for shape comparison need not conform strictly to the dimensions of the broken mandible under consideration, indicates the generality of our method.

Fig. 4 and Table 3 compare the performance of the ICP, Geometric and Geometric-ICP algorithms. In Fig. 4 (where the results of registration are shown for dataset 1), it is observed that the ICP and Geometric-ICP algorithms perform better than the Geometric algorithm. Table 3 shows a detailed quantitative comparison of the performance of these algorithms for five different

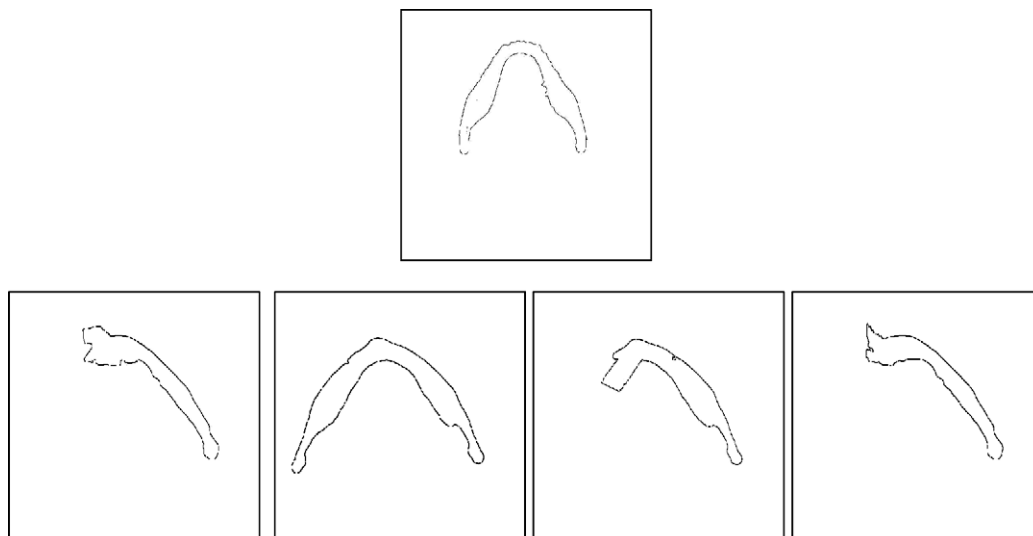


Fig. 3. Reference contour in the first row and 4 coarsely registered competing contours in the second row.



Fig. 4. Slice-wise reconstruction using the ICP, Geometric and Geometric-ICP algorithms displayed in first, second and third rows, respectively.

Table 3

A performance comparison of the three different reconstruction algorithms.

Dataset	Algorithm	MSE (mm ²)	No. of iterations for convergence
1	ICP	2.07	8
1	Geometric	4.57	2
1	Geometric-ICP	1.96	3
2	ICP	2.09	8
2	Geometric	4.51	2
2	Geometric-ICP	1.95	4
3	ICP	3.49	10
3	Geometric	4.55	2
3	Geometric-ICP	1.91	4
4	ICP	3.56	10
4	Geometric	4.53	2
4	Geometric-ICP	2.03	3
5	ICP	3.53	14
5	Geometric	4.60	2
5	Geometric-ICP	2.23	4

datasets. The Geometric algorithm performs only a coarse registration based on a few pairs of points. So, the resulting MSE from this algorithm is higher compared to that resulting from both the ICP

and the Geometric-ICP algorithms. The Geometric-ICP algorithm outperforms the ICP algorithm because of a better initialization. The actual registration in each of the algorithms is performed between two fracture surfaces, which are essentially 3D datasets. For the purpose of illustration, we display the results of the reconstruction in consecutive 2D CT image slices (Fig. 4). Our results also illustrate that the proposed Geometric-ICP algorithm not only yields a lower MSE value compared to the original ICP algorithm, but also converges in fewer iterations compared to the ICP algorithm. The mean and standard deviation of MSE for ICP, Geometric and Geometric-ICP algorithms, calculated in mm, from the five datasets, are found to be: 2.95 ± 0.79 , 4.56 ± 0.03 and 2.02 ± 0.13 , respectively. The reduction in the MSE between the ICP and the Geometric-ICP algorithms, on average, is quite critical from the viewpoint of surgical reconstruction. This is because a very small error in the fracture surface registration can result in an unacceptably large error in the overall alignment of the two bone fragments.

10. Conclusions and future work

The problem of virtual craniofacial reconstruction is modeled as one of rigid surface registration. We have presented significant enhancements to the conventional ICP-based registration procedure based on the incorporation of graph theory and geometric constraints. MCMW matching for a bipartite graph is used to

establish the necessary correspondence in the ICP algorithm, thus obviating the need for any prior alignment between the fracture surfaces. After treating the bounding box of each fracture surface as a cycle graph, the rotational and reflectional automorphs (of one of the cycle graphs) are constructed to generate possible initial states for the ICP algorithm. Rigid transformation-invariant local geometric constraints and shape-based global geometric constraints are applied successively to yield the best initial state for the ICP algorithm. Initialization of the conventional ICP algorithm with a geometrically accurate transformation results in improved accuracy and faster convergence.

As a part of future research, we plan to replace the bounding box of the fracture surface with the convex hull. This could potentially allow the enforcement of stronger geometric constraints, resulting in more accurate registration in more complex scenarios such as multiple fractures. Another direction for future research is to apply the proposed method to other forms of reconstructive surgery such as orthopedic surgery.

Acknowledgments

The research was partially supported by research grants from the Biomedical and Health Sciences Institute (BHSI), Faculty of Engineering (FOE) and the University of Georgia Research Foundation (UGARF) at the University of Georgia, Athens, Georgia. We sincerely thank the anonymous reviewers for their insightful comments, which have significantly improved the quality of this paper.

References

- Besl, P.J., McKay, N.D., 1992. A method for registration of 3-D shapes. *IEEE Trans. Pattern Anal. Machine Intell.* 14 (2), 239–256.
- Bhandarkar, S.M., Chowdhury, A.S., Tang, Y., Yu, J.C., Tollner, E.W., 2007a. Computer vision guided virtual craniofacial reconstruction. *Comput. Med. Image Graph.* 31 (6), 418–427.
- Bhandarkar, S.M., Chowdhury, A.S., Robinson, R.W., Yu, J.C., 2007b. Novel graph theoretic enhancements to ICP-based virtual craniofacial reconstruction. In: *Proc. fourth IEEE Internat. Sympos. on Biomedical Imaging (ISBI)*, pp. 1136–1139.
- Cevidane, L.H.S., Styner, M., Phillips, C., Oliveira, A.E.F., Tulloch, J.F.C., 2007. 3D morphometric changes 1 year after jaw surgery. In: *Proc. fourth IEEE Sympos. on Biomedical Imaging (ISBI)*, Metro Washington, DC, pp. 1332–1335.
- Christofides, N., 1975. *Graph Theory an Algorithmic Approach*. Academic Press.
- Cormen, T.H., Leiserson, C.E., Rivest, R.L., Stein, C., 2001. *Introduction to Algorithms*. MIT Press.
- Enciso, R., Memon, A., Neumann, U., Mah, J., 2003. The virtual cranio-facial patient project: 3d modelling and animation. In: J.D. Westwood, J.D., Hoffman, H.M., Mogel, G.T., Phillips, R., Robb, R.A., Stredney, D. (Eds.), *Proc. 11th 'Medicine Meets Virtual Reality' Conf.*, Newport Beach, USA, pp. 65–72.
- Granger, S., Pennec, X., Roche, A., 2001. Rigid point-surface registration using an EM variant of ICP for computer guided oral implantology. In: *Proc. fourth Internat. Conf. on Medical Image Computing and Computer Assisted Intervention (MICCAI)*, LNCS 2208, Utrecht, The Netherlands, pp. 752–761.
- Hamilton, W.R., 1847. On quaternions. *Proc. Royal Ir. Acad.* 3, 1–16.
- Huttenlocher, D.P., Klanderma, G.A., Rucklidge, W.J., 1993. Comparing images using the hausdorff distance. *IEEE Trans. Pattern Anal. Machine Intell.* 15 (9), 850–863.
- Kim, W., Kak, A.C., 1991. 3-D object recognition using bipartite matching embedded in discrete relaxation. *IEEE Trans. Pattern Anal. Machine Intell.* 13 (3), 224–251.
- King, R.E., Scianna, J.M., Petruzzelli, G.J., 2004. Mandible fracture patterns: A suburban trauma center experience. *Am. J. Otolaryngol.* 25 (5), 301–307.
- Kuhn, H.W., 1955. The Hungarian method for the assignment problem. *Nav. Res. Log. Quart.* 2.
- Mollemans, W., Schutyser, F., Nadjmi, N., Suetens, P., 2005. Very fast soft tissue predictions with mass tensor model for maxillofacial surgery planning systems. In: *Proc. ninth Annual Conf. of the Internat. Soc. for Computer Aided Surgery*, pp. 491–496.
- Nakajima, H., Kaneko, T., Kurihara, T., Fujino, T., 2001. Craniofacial surgical simulation in the 3-dimensional CT SurgiPlan system. *Keio J. Med.* 50 (2), 95–102.
- Ogundare, B.O., Bonnick, A., Bayley, N., 2003. Pattern of mandibular fractures in an urban major trauma center. *J. Oral Maxillofac. Surg.* 61 (6), 713–718.
- Papadimitriou, C.H., Steiglitz, K., 1982. *Combinatorial Optimization: Algorithms and Complexity*. Prentice Hall of India.
- Patel, V.V., Vannier, M.W., Marsh, J.L., Lo, L.J., 1996. Assessing craniofacial surgical simulation. *IEEE Comput. Graph Appl.* 16 (1), 46–54.
- Sahoo, P.K., Soltani, S., Wong, K.C., Chen, Y.C., 1988. A survey of thresholding techniques. *Comput. Vision Graphics Image Process.* 41, 233–260.
- Siessegger, M., Schneider, B.T., Mischkowski, R.A., Lazar, F., Krug, B., Klesper, B., Zoller, J.E., 2001. Use of an image-guided navigation system in dental implant surgery in anatomically complex operation sites. *J. Craniomaxillofac. Surg.* 29 (5), 276–281.
- Valiente, G., 2002. *Algorithms on Trees and Graphs*. Springer-Verlag, Berlin-Heidelberg.
- Veltkamp, R.C., Latecki, L.J., 2006. Properties and performance of shape similarity measures. In: *Proc. 10th IFCS Internat. Conf. on Data Science and Classification*, Ljubljana, Slovenia, pp. 1–9.
- Wang, Y., Peterson, B., Staib, L., 2000. Shape-based 3-D surface correspondence using geodesics and local geometry. In: *Proc. first IEEE Internat. Conf. on Computer Vision and Pattern Recognition (CVPR)*, vol. II, Hilton Head Island, SC, pp. 644–651.